Modeling and Validation of a Complex Vehicle Dynamics Model for Real-time Applications

Peter Riegl and Andreas Gaull

Carissma, Ingolstadt Univ. of Applied Sciences, Esplanade 10, Ingolstadt, Germany

Keywords: Vehicle Dynamics, Twin Track Model, Real-time, Tire Model, Magic Formula.

Abstract: This paper deals with the modeling and validation of a complex vehicle dynamics model implemented in Matlab, which should enable real-time simulation. In detail, the powertrain and the tire model Magic Formula by Pacejka are presented. In addition to the horizontal dynamics, which can also be found in single track models, the here presented vehicle model also takes into account the vertical motion as well as the pitch and roll behavior. Furthermore, the wheel load fluctuations during the driving maneuvers are included. The equations of motion are based on multi-body dynamics. Based on three driving scenarios, which are simulated in the software CarMaker, the quality of the driving dynamics model is evaluated.

1   INTRODUCTION

In addition to the passive safety of a vehicle aimed at reducing the consequences of a traffic accident, active vehicle safety has become increasingly important in recent years. The main goal of active safety systems is to detect possible dangers in advance with the help of electronic vehicle control systems and to initiate countermeasures by means of targeted interventions on the vehicle motion in order to avoid collisions. Another development trend is the autonomous driving. Here vehicle control systems take over the control of the vehicle during steering, braking and acceleration maneuvers, without human intervention being necessary. For this, the current vehicle parameters have to be known. Furthermore, information about the position of the vehicle relative to the road and about other road users is needed. This data have be identified by suitable sensors like GPS, cameras or Lidar. Both, active vehicle safety and autonomous driving require control algorithms that process the provided sensor data in real-time and perform corresponding control interventions. For the development and the testing of such control systems in critical situations real-time vehicle dynamics models are necessary, which take into account all important influences on the vehicle handling with a sufficient accuracy. This is not always guaranteed in the case of simplistic models used so far in many studies like single track models and twin track models, whose center of gravity is on the road level. Therefore, it is necessary to develop a nonlinear

twin track model, which also takes into account the vertical dynamics with the occurring pitch and roll of the vehicle body. This model should indicate the same behavior as complex systems like CarMaker that used for validation.

2   NONLINEAR TWIN TRACK MODEL

2.1   Kinematics

The kinematics of the vehicle body can be described by means of three translational x_V, y_V, z_V and three rotational degrees of freedom φ, θ, ψ. Furthermore, each wheel performs a rotation ρ_j about its wheel-carrier-fixed axis. In this paper, the index j indicates the components front left, front right, rear left or rear right. The suspension, whose exact kinematics is disregarded here, enables a vertical motion of the wheel. The tire deflection z_{W_j} results from the wheel load changes and the road bumps. Thus, the vehicle model has in total 14 degrees of freedom (cf. figure 1). To describe the equations of motion, the generalized coordinates and generalized velocities are summarized as state vectors (Schramm et al., 2018):

$$\boldsymbol{z} = \left[x_V, y_V, z_V, \varphi, \theta, \psi, z_{W_{fl}}, z_{W_{fr}}, z_{W_{rl}}, z_{W_{rr}}, \right.$$
$$\left. \rho_{fl}, \rho_{fr}, \rho_{rl}, \rho_{rr} \right]^T = \left[{}_I \boldsymbol{r}_{IV}, \boldsymbol{\Phi}_{IV}, \boldsymbol{z}_W, \boldsymbol{\rho} \right]^T \quad (1)$$
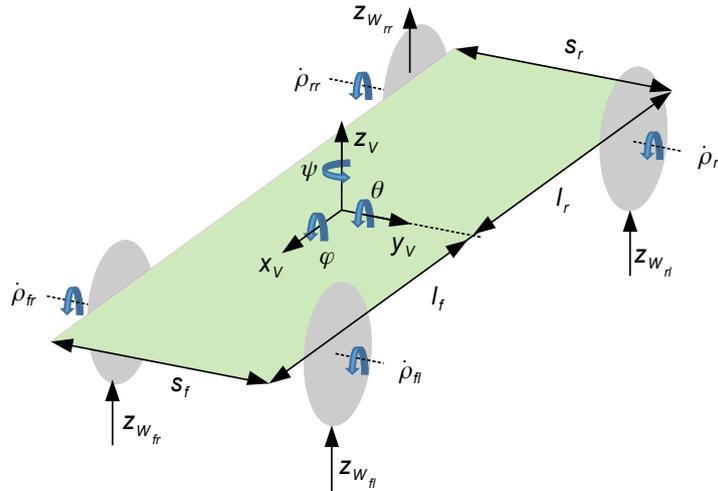
403

Figure 1: Vehicle model.

$$\boldsymbol{u} = \left[v_x, v_y, v_z, \omega_x, \omega_y, \omega_z, \dot{z}_{W_{fl}}, \dot{z}_{W_{fr}}, \dot{z}_{W_{rl}}, \dot{z}_{W_{rr}}, \right.$$
$$\left. \dot{\rho}_{fl}, \dot{\rho}_{fr}, \dot{\rho}_{rl}, \dot{\rho}_{rr} \right]^T = \left[_V\boldsymbol{v}_{IV}, _V\boldsymbol{\omega}_{IV}, \dot{z}_W, \dot{\boldsymbol{\rho}} \right] \quad (2)$$

The vehicle is controlled by an input vector $\boldsymbol{q}$ which consists of the steering wheel angle δ_{SW}, the position of the accelerator pedal α_A, the position of the brake pedal α_B and the position of the clutch pedal α_C

$$\boldsymbol{q} = \left[\delta_{SW}, \alpha_A, \alpha_B, \alpha_C \right]^T. \quad (3)$$

The motion of the vehicle body and the wheels relative to the inertial system I is described by body-fixed reference frames. The coordinate system of the vehicle body is denoted by V. The kinematics of each wheel is represented by a reference frame W_j. The rotation of the vehicle body with respect to the inertial system is described by the three elementary rotations with respect to the body-fixed axes z_V, y_V and x_V. The corresponding matrix is

$$\boldsymbol{A}_{IV} = \boldsymbol{A}_z(\psi) \cdot \boldsymbol{A}_y(\theta) \cdot \boldsymbol{A}_x(\varphi). \quad (4)$$

The angular velocity is calculated in the coordinate system of the vehicle body

$$_V\boldsymbol{\omega}_{IV} = \dot{\boldsymbol{\varphi}} + \boldsymbol{A}_x^T \cdot \dot{\boldsymbol{\theta}} + \boldsymbol{A}_x^T \cdot \boldsymbol{A}_y^T \cdot \dot{\boldsymbol{\psi}} = \boldsymbol{A}_{\omega} \cdot \dot{\boldsymbol{\Phi}}_{IV}$$
$$= \begin{bmatrix} 1 & 0 & -\sin(\theta) \\ 0 & \cos(\varphi) & \sin(\varphi) \cdot \cos(\theta) \\ 0 & -\sin(\varphi) & \cos(\varphi) \cdot \cos(\theta) \end{bmatrix} \cdot \begin{bmatrix} \dot{\varphi} \\ \dot{\theta} \\ \dot{\psi} \end{bmatrix}. \quad (5)$$

The motion of the wheels relative to the inertial frame, not including their own rotation about the wheels axis, is described by a rotation matrix. For the steered front wheels, this results in

$$\boldsymbol{A}_{VW_{fl}} = \boldsymbol{A}_{VW_{fr}} = \boldsymbol{A}_x^T(\varphi) \cdot \boldsymbol{A}_y^T(\theta) \cdot \boldsymbol{A}_z(\delta). \quad (6)$$

For the rear wheels correspondingly, it holds

$$\boldsymbol{A}_{VW_{rl}} = \boldsymbol{A}_{VW_{rr}} = \boldsymbol{A}_x^T(\varphi) \cdot \boldsymbol{A}_y^T(\theta). \quad (7)$$

The steering angle of the front wheels δ results from the steering gear ratio i_{SG} and the steering wheel angle δ_{SW}, which is provided as an input signal

$$\delta = i_{SG} \cdot \delta_{SW}. \quad (8)$$

For the sake of simplicity, i_{SG} is assumed to be constant. The current position of the center of mass of the vehicle body relative to the origin of the inertial system is described by the vector $_I\boldsymbol{r}_{IV}$

$$_I\boldsymbol{r}_{IV} = [x_V, y_V, z_V]^T. \quad (9)$$

The translational velocity then yields in the reference frame of the vehicle body

$$_V\boldsymbol{v}_{IV} = \begin{bmatrix} v_x \\ v_y \\ v_z \end{bmatrix} = \boldsymbol{A}_{IV}^T \cdot \begin{bmatrix} \dot{x}_V \\ \dot{y}_V \\ \dot{z}_V \end{bmatrix} = \boldsymbol{A}_{IV}^T \cdot {}_I\dot{\boldsymbol{r}}_{IV}. \quad (10)$$

Finally, the translational acceleration results in

$$_V\boldsymbol{a}_{IV} = {}_V\dot{\boldsymbol{v}}_{IV} + {}_V\tilde{\boldsymbol{\omega}}_{IV} \cdot {}_V\boldsymbol{v}_{IV}. \quad (11)$$

The kinematic equation of motion provides a relationship between the time derivative of the state variables $\dot{\boldsymbol{z}}$ and the state variables at the velocity level

$$\boldsymbol{u} = \begin{bmatrix} \boldsymbol{A}_{IV}^T & \boldsymbol{0} & \boldsymbol{0} & \boldsymbol{0} \\ \boldsymbol{0} & \boldsymbol{A}_{\omega} & \boldsymbol{0} & \boldsymbol{0} \\ \boldsymbol{0} & \boldsymbol{0} & \boldsymbol{E} & \boldsymbol{0} \\ \boldsymbol{0} & \boldsymbol{0} & \boldsymbol{0} & \boldsymbol{E} \end{bmatrix} \cdot \begin{bmatrix} _I\dot{\boldsymbol{r}}_{IV} \\ \dot{\boldsymbol{\Phi}}_{IV} \\ \dot{z}_W \\ \dot{\boldsymbol{\rho}} \end{bmatrix} = \boldsymbol{K} \cdot \dot{\boldsymbol{z}}. \quad (12)$$

2.2 Dynamics

After having presented the kinematics of the vehicle body in the previous section, the dynamic equations of motion based on the conservation of momentum and the angular momentum are introduced. The corresponding equations are

$$m_V \cdot (_V\dot{\boldsymbol{v}}_{IV} + _V\tilde{\boldsymbol{\omega}}_{IV} \cdot _V\boldsymbol{v}_{IV})$$
$$= \sum_j {_V}\boldsymbol{F}_j - m_V \cdot \boldsymbol{A}_{VI} \cdot _I\boldsymbol{e}_z \cdot g + _V\boldsymbol{F}_{DR} \quad (13)$$

$$_V\boldsymbol{\Theta}_V \cdot _V\dot{\boldsymbol{\omega}}_{IV} + _V\tilde{\boldsymbol{\omega}}_{IV} \cdot (_V\boldsymbol{\Theta}_V \cdot _V\boldsymbol{\omega}_{IV})$$
$$= \sum_j {_V}\tilde{\boldsymbol{r}}_{VB_j} \cdot _V\boldsymbol{F}_j + _V\boldsymbol{M}_{DR}. \quad (14)$$

The forces and torques occurring in the equations of motion (13) and (14) will be described in more detail in the next chapters. The vector $_I\boldsymbol{e}_z$ represents the vertical coordinate unit vector. The driving resistances $_V\boldsymbol{F}_{DR}$ counteract the motion of the vehicle. The forces acting from the suspension $_V\boldsymbol{F}_{FD_j}$ and its associated wheel $_V\boldsymbol{F}_{W_j}$ to the vehicle body are summarized in

$$_V\boldsymbol{F}_j = _V\boldsymbol{F}_{FD_j} + _V\boldsymbol{F}_{W_j}. \quad (15)$$

The wheel forces in vertical and horizontal direction are presented in chapter 6. The vector $_V\boldsymbol{r}_{VB_j}$ indicates the distance between the force application point of the wheel suspension and the center of gravity of the vehicle body. $_V\boldsymbol{M}_{DR}$ is the driving resistance torque. The wheels and wheel carriers can be excited to vibrations by road bumps s_{W_j}. For this purpose, the principle of linear momentum in the vertical direction of the inertial frame is needed

$$m_{W_j} \cdot \ddot{z}_{W_j} = F_{z_j} - F_{FD_j} - m_{W_j} \cdot g$$
$$+ C_{W_j} \cdot s_{W_j} + D_{W_j} \cdot \dot{s}_{W_j}. \quad (16)$$

The stiffness C_{W_j} and the damping D_{W_j} characterize the behavior of the tire in the vertical direction.
The angular acceleration of the wheel in figure 2 results from the angular momentum conservation in the wheel-fixed frame of reference. The torque acting on a wheel is determined from the difference between the driving torque M_{A_j} and the torques counteracting the rotational motion. These are the braking torque M_{B_j}, the rolling resistance torque M_{Wy_j} and the torque caused by the tire longitudinal force F_{Wx_j} and its static radius r_{stat_j}

$$\Theta_{Wy_j} \cdot \ddot{\rho}_j = M_{A_j} - M_{B_j} - M_{Wy_j} - r_{stat_j} \cdot F_{Wx_j}. \quad (17)$$

The current braking torque is proportional to the brake pedal position α_B and the maximum transmissible torque at the brake disc $M_{B_{max\_j}}$

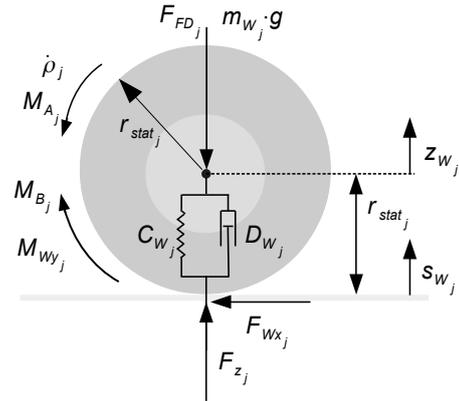$$M_{B_j} = M_{B_{max\_j}} \cdot \alpha_B. \quad (18)$$

Figure 2: Wheel dynamics.

3 DRIVING RESISTANCE

The driving resistance force $_V\boldsymbol{F}_{DR}$ counteracts the motion of the vehicle and thus determines the driving torque, which is needed to achieve the desired driving condition. It is composed of the air resistance $_V\boldsymbol{F}_{AR}$ and the climbing resistance $_V\boldsymbol{F}_{CR}$

$$_V\boldsymbol{F}_{DR} = _V\boldsymbol{F}_{AR} + _V\boldsymbol{F}_{CR}. \quad (19)$$

The acceleration resistance $_V\boldsymbol{F}_{ACR}$ is not explicitly considered here. However, the model of powertrain includes all rotational inertias that oppose a change of speed. The climbing resistance depends on the slope angle α_{Sa} of the road

$$_V\boldsymbol{F}_{CR} = -m_V \cdot sin(\alpha_{Sa}) \cdot g \cdot \boldsymbol{A}_{VI} \cdot _I\boldsymbol{e}_z. \quad (20)$$

The aerodynamic forces and torques acting on the outer skin of the vehicle body are based on the friction resistance, the internal resistance and the form resistance. The latter one represents the majority with a share of 85% (Popp and Schiehlen, 1993) and is considerd in this vehicle model. Due to the geometry of the outer skin, the previously laminar air flow at the rear of the vehicle becomes turbulent. The energy dissipation caused by the occurring vortex structures is then reflected in the driving resistance. The air forces are proportional to the dynamic pressure

$$p_D = \rho_A \cdot \frac{\|_I\boldsymbol{v}_{rel}\|^2}{2}; \quad (21)$$

with the air density ρ_A. The relative velocity $_I\boldsymbol{v}_{rel}$ between the vehicle $_I\boldsymbol{v}_{IV}$ and the airflow $_I\boldsymbol{v}_A$ is defined in the inertial system

$$_I\boldsymbol{v}_{rel} = _I\boldsymbol{v}_A + _I\boldsymbol{v}_{IV} = _I\boldsymbol{v}_A + \boldsymbol{A}_{IV} \cdot _V\boldsymbol{v}_{IV}. \quad (22)$$

The vector of the air forces results from

$$_V\boldsymbol{F}_{AR} = -_V\boldsymbol{c}_d \cdot A \cdot p_D = -_V\boldsymbol{c}_d \cdot A \cdot \rho_A \cdot \frac{\|_I\boldsymbol{v}_{rel}\|^2}{2}; \quad (23)$$

with the effective cross-sectional area of the vehicle A and the angle-dependent vector of the drag coefficients $_V\boldsymbol{c}_d$, which is defined in the vehicle body frame. The torque that is generated by the aerodynamic forces on the vehicle body acts at the pressure point D and is given by

$$_V\boldsymbol{M}_{AR} = _V\tilde{\boldsymbol{r}}_{VD} \cdot _V\boldsymbol{F}_{AR} \qquad (24)$$

and is equal to the driving resistance torque

$$_V\boldsymbol{M}_{DR} = _V\boldsymbol{M}_{AR}. \qquad (25)$$

The rolling resistance torque counteracts the motion of the wheels. It results from the tire model and corresponds to the torque around the wheel axis M_{Wy} and is considered in the wheel dynamics (17).

4 SUSPENSION FORCES

The forces acting between the vehicle body and the suspension determine the dynamics of the vehicle and are caused by the suspension springs, the suspension dampers and the stabilizers

$$_V\boldsymbol{F}_{FD_j} = _V\boldsymbol{F}_{F_j} + _V\boldsymbol{F}_{D_j} + _V\boldsymbol{F}_{S_j}. \qquad (26)$$

The basis for the three force components is the relative motion between the connection point of the force elements on the vehicle body and the wheel center whose vertical motion z_{W_j} results from the compliance of the tire due to the wheel load changes. The vertical motion of the force application point of a suspension on the vehicle body is calculated in the inertial frame I

$$_I\boldsymbol{r}_{IB_j} = \begin{bmatrix} 0 \\ 0 \\ z_V \end{bmatrix} + \boldsymbol{A}_{IV} \cdot _V\boldsymbol{r}_{VB_j}. \qquad (27)$$

The vector $_V\boldsymbol{r}_{VB_j}$ indicates the distance between the reference frame of the vehicle body and the wheel force application point B_j. The suspension of the right rear wheel is shown in figure 3. The remaining suspensions are modelled analogously. The related components are

$$_V\boldsymbol{r}_{VB_{fl}} = \begin{bmatrix} l_f \\ \frac{s_f}{2} \\ -s_z \end{bmatrix}, \quad _V\boldsymbol{r}_{VB_{fr}} = \begin{bmatrix} l_f \\ -\frac{s_f}{2} \\ -s_z \end{bmatrix},$$

$$_V\boldsymbol{r}_{VB_{rl}} = \begin{bmatrix} -l_r \\ \frac{s_r}{2} \\ -s_z \end{bmatrix}, \quad _V\boldsymbol{r}_{VB_{rr}} = \begin{bmatrix} -l_r \\ -\frac{s_r}{2} \\ -s_z \end{bmatrix}. \qquad (28)$$

The spring force is composed of a force law $f(l_F)$ and the associated force direction $\boldsymbol{e}_F$

$$\boldsymbol{F}_F = f(l_F) \cdot \frac{\boldsymbol{l}_F}{l_F} = f(l_F) \cdot \boldsymbol{e}_F. \qquad (29)$$
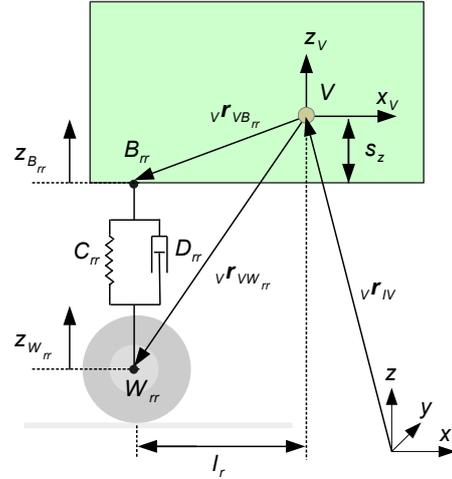

Figure 3: Suspension of the right rear wheel.

The direction of force is assumed to be perpendicular to the road surface. For this reason, only the vertical component of the vector $z_{B_j} = _I\boldsymbol{r}_{IB_j}(3)$ is used in the calculation of the spring force. The current length of the suspension spring results from the vertical motion of the attachment point on the vehicle body z_{B_j}, the position of wheel center point z_{W_j} and the static spring length l_{stat_j}

$$l_{F_j} = z_{B_j} - z_{W_j} + l_{stat_j}. \qquad (30)$$

For example, the spring force of the left front wheel with the relaxed spring length $l_{0_{fl}}$ yields to

$$_V\boldsymbol{F}_{F_{fl}} = -\boldsymbol{A}_{VI} \cdot C_{fl} \cdot \begin{bmatrix} 0 \\ 0 \\ z_{B_{fl}} - z_{W_{fl}} + l_{stat_{fl}} - l_{0_{fl}} \end{bmatrix}$$

$$= \boldsymbol{A}_{VI} \cdot \begin{bmatrix} 0 \\ 0 \\ -C_{fl} \cdot (z_{B_{fl}} - z_{W_{fl}}) + \frac{l_r \cdot m_V \cdot g}{2 \cdot l} \end{bmatrix} \qquad (31)$$

The velocity of the attachment point of the suspension at the vehicle body is composed of the velocity of the vehicle body and a component resulting from its angular velocity

$$_I\boldsymbol{v}_{IB_j} = _I\boldsymbol{v}_{IV} + _I\tilde{\boldsymbol{\omega}}_{IV} \cdot _I\boldsymbol{r}_{VB_j}. \qquad (32)$$

In analogy to the spring force, only the vertical component is considered in the calculation of the damper force. This results with $\dot{z}_{B_j} = _I\boldsymbol{v}_{IB_j}(3)$ in

$$_V\boldsymbol{F}_{D_j} = -\boldsymbol{A}_{VI} \cdot D_j \cdot \begin{bmatrix} 0 \\ 0 \\ \dot{z}_{B_j} - \dot{z}_{W_j} \end{bmatrix}. \qquad (33)$$

Due to the different deflection of the left and right wheel of an axle, a force is induced in the roll stabilizer, which tries to compensate this difference. For

the front and rear axle this leads to

$$_V\boldsymbol{F}_{S_{fl}} = -_V\boldsymbol{F}_{S_{fr}} = -\boldsymbol{A}_{VI} \cdot C_{S_f} \cdot \begin{bmatrix} 0 \\ 0 \\ l_{F_{fl}} - l_{F_{fr}} \end{bmatrix} ; \quad (34)$$

$$_V\boldsymbol{F}_{S_{rl}} = -_V\boldsymbol{F}_{S_{rr}} = -\boldsymbol{A}_{VI} \cdot C_{S_r} \cdot \begin{bmatrix} 0 \\ 0 \\ l_{F_{rl}} - l_{F_{rr}} \end{bmatrix} . \quad (35)$$

The calculation of the tire slip resulting from the tire-road contact requires the current position and the speed of the wheel center. These kinematic variables are described in the reference frame of the vehicle body.

$$_V\boldsymbol{r}_{VW_j} = _V\boldsymbol{r}_{VB_j} - \boldsymbol{A}_{VI} \cdot \begin{bmatrix} 0 \\ 0 \\ l_{F_j} \end{bmatrix} \quad (36)$$

$$_V\boldsymbol{v}_{IW_j} = _V\boldsymbol{v}_{IV} + _V\tilde{\boldsymbol{\omega}}_{IV} \cdot _V\boldsymbol{r}_{VW_j} - \boldsymbol{A}_{VI} \cdot \begin{bmatrix} 0 \\ 0 \\ \dot{z}_{B_j} - \dot{z}_{W_j} \end{bmatrix}$$

The computation of the tire slip, however, takes place in the wheel-fixed reference frame, such that

$$_W\boldsymbol{v}_{IW_j} = \boldsymbol{A}_{WV_j} \cdot _V\boldsymbol{v}_{IW_j} \quad (37)$$

is needed.

5 POWERTRAIN

To determine the temporal change of the angular velocity of the driven wheels, the components of the powertrain are needed. As an input only the desired position of the accelerator pedal is to be specified, which corresponds to the position of the throttle valve. The behavior of the engine is described by the full load characteristic and the speed-dependent curve of the drag torque, which represents the friction losses in the engine. The actual usable range is limited by the idle speed. No torque can be transmitted below this limit. The full load characteristic indicates the torque that is available at the maximum accelerator pedal position ($\alpha_A = 1$). In most driving situations, however, a lower torque is provided which can be approximated using a nonlinear relationship

$$M_E = M_{Drag} \cdot (1 - \alpha_A^n) + M_{Full\_Load} \cdot \alpha_A^n. \quad (38)$$

The exponent n defines the characteristic of the curve. The different shape types are listed in table 1. Taking into account the mass moment of inertia of the engine Θ_E, the torque transmitted to the input shaft of the clutch yields to

$$M_C = M_E - \Theta_E \cdot \dot{\omega}_E. \quad (39)$$

Table 1: Shape of the engine torque curve.

- $n = 1 \rightarrow$ linear
- $n < 1 \rightarrow$ root shaped
- $n > 1 \rightarrow$ parabolic

The clutch consists of two discs (cf. figure 4). The input clutch disk with the moment of inertia Θ_{Cin} is connected to the crankshaft and thus rotates with the angular velocity of the engine ω_E. The output clutch shaft, which has a moment of inertia Θ_{Cout}, may show a different angular velocity ω_C during the shifting process. Since the shifting times are regarded as short compared to the entire simulation time, it is assumed that both clutch discs always have the same velocity. The torque transmitted by the clutch is directly proportional to the position of the clutch pedal α_C. A fully actuated clutch ($\alpha_C = 1$) ensures that the engine is decoupled from the rest of the drive and no more engine torque is transmitted. If the clutch is not actuated, the entire engine torque acts on the output clutch disc. The torque transmitted to the gearbox results in

$$M_G = \left(M_C - \Theta_{Cin} \cdot \dot{\omega}_E \right) \cdot (1 - \alpha_C) - \Theta_{Cout} \cdot \dot{\omega}_C. \quad (40)$$

The gearbox consists of a manual transmission, a transfer case and an axle drive. The rotating masses of the gearbox are combined in two mass moments of inertia. The transmission input shaft, together with the gears mounted thereon, has the rotational inertia Θ_{Gin}. Due to the gear ratio i_G, the transmission output shaft with the mass moment of inertia Θ_{Gout} has a different angular velocity ω_G

$$\omega_C = i_G \cdot \omega_G. \quad (41)$$

The torque transmitted from the gearbox to the transfer case is given by

$$M_D = \left(M_G - \Theta_{Gin} \cdot \dot{\omega}_C \right) \cdot i_G - \Theta_{Gout} \cdot \dot{\omega}_G. \quad (42)$$

The transfer case distributes the generated torque to the axles to be driven. The difference between the several drive configurations is defined by a parameter α_V. If the vehicle has a front-wheel drive, the value is zero. A rear-wheel drive uses $\alpha_V = 1$. The all-wheel drive has a value in between. The axle drive with the ratio i_D is the last component of the powertrain. It ensures that the same torque M_A is transmitted to the inner and outer wheels when cornering. The angular velocity of the driven wheels can be determined from

$$\omega_G = i_D \cdot \omega_D = \frac{i_D}{2} \cdot (\omega_l + \omega_r). \quad (43)$$

The corresponding torque results in

$$M_A = \frac{\left(M_D - \Theta_{Din} \cdot \dot{\omega}_G \right) \cdot i_D - \Theta_{Dout} \cdot \dot{\omega}_D}{2}. \quad (44)$$
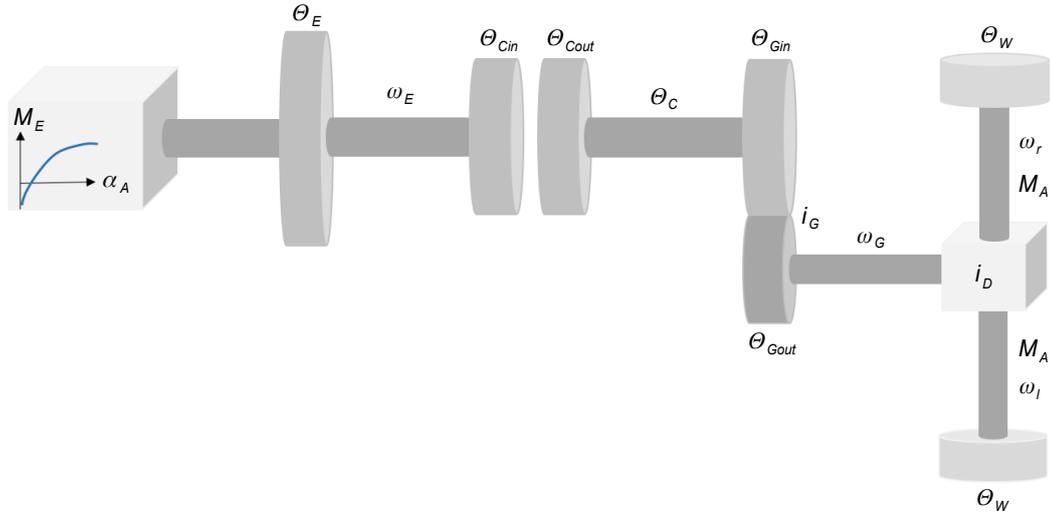
Figure 4: Powertrain.

The driving torque acting on a front wheel is

$$M_{A_k} = (1 - \alpha_V) \cdot M_A \quad k = fl, fr. \tag{45}$$

The torque that drives a rear wheel is given by

$$M_{A_m} = \alpha_V \cdot M_A \quad m = rl, rr. \tag{46}$$

After the single components have been described, they are assembled into an overall system. For this the equations (39), (40), (42) and (44) are needed. With (41) and (43) the angular velocity can be converted. The total torque can be divided into two components

$$M_{tot} = 2 \cdot M_A = M_{PT} - \Theta_{tot} \cdot \dot{\omega}_D. \tag{47}$$

The first component represents the torque provided by the engine

$$M_{PT} = M_E \cdot (1 - \alpha_C) \cdot i_G \cdot i_D \tag{48}$$

and the second component considers the total mass moment of inertia of the powertrain, which counteracts a change of the angular velocity

$$\Theta_{tot} = \left[\left((\Theta_E + \Theta_{Cin}) \cdot (1 - \alpha_C) + \Theta_{Cout} \right. \right.$$
$$\left. \left. + \Theta_{Gin} \right) \cdot i_G^2 + \Theta_{Gout} + \Theta_{Din} \right] \cdot i_D^2 + \Theta_{Dout}. \tag{49}$$

The mass moment of inertia reduced to a wheel of the front axle consists of the rotational inertia of the front wheel θ_{W_f} and a component resulting from the powertrain

$$\Theta_{totW_k} = \Theta_{W_f} + \frac{1 - \alpha_V}{2} \cdot \Theta_{tot} \quad k = fl, fr. \tag{50}$$

The total rotational mass moment of inertia of a rear wheel results in

$$\Theta_{totW_m} = \Theta_{W_r} + \frac{\alpha_V}{2} \cdot \Theta_{tot} \quad m = rl, rr. \tag{51}$$

6 TIRE BEHAVIOR

6.1 Wheel Load

The wheel load F_{z_j} consists of two components. The static component results from the mass distribution of the vehicle body m_V and the weight of a wheel and its associated wheel carrier, which are summarized in $m_{W_j} \cdot g$. The dynamic component considers the loads that arise in the suspensions as a result of the pitch and roll of the vehicle body:

$$F_{z_{fl}} = \left(\frac{m_V \cdot l_r}{2 \cdot l} + m_{W_f} \right) \cdot g - C_{fl} \cdot z_{fl} - D_{fl} \cdot \dot{z}_{fl}$$

$$F_{z_{fr}} = \left(\frac{m_V \cdot l_r}{2 \cdot l} + m_{W_f} \right) \cdot g - C_{fr} \cdot z_{fr} - D_{fr} \cdot \dot{z}_{fr}$$

$$F_{z_{rl}} = \left(\frac{m_V \cdot l_f}{2 \cdot l} + m_{W_r} \right) \cdot g - C_{rl} \cdot z_{rl} - D_{rl} \cdot \dot{z}_{rl}$$

$$F_{z_{rr}} = \left(\frac{m_V \cdot l_f}{2 \cdot l} + m_{W_r} \right) \cdot g - C_{rr} \cdot z_{rr} - D_{rr} \cdot \dot{z}_{rr} \tag{52}$$

The parameter l_f and l_r denote the distance between the center of gravity of the vehicle body and the front and rear axle. The wheelbase is characterized by l. The spring deflection results from the relative motion between the attachment point of the wheel suspension at the vehicle body z_{B_j} and the tire deflection z_{W_j}.

$$z_j = z_{B_j} - z_{W_j} \tag{53}$$

$$\dot{z}_j = \dot{z}_{B_j} - \dot{z}_{W_j} \tag{54}$$

6.2 Horizontal Wheel Force

For the transmission of the horizontal forces in the contact area between the tire and the road, friction is necessary. The most important physical effects that are responsible for those forces are adhesion and hysteresis friction (Gillespie, 1992). The first component is based on intermolecular bonding between the rubber of the tire and the road surface. The second part results in a form fit due to meshing of the tire contact patch and the road surface. Pure longitudinal forces F_{Wx_j} only appear when driving straight ahead. Pure lateral forces F_{Wy_j} occur for freely rolling wheels. In all other driving situations, there is a superposition of the two forces. The maximum transmissible horizontal forces in the tire longitudinal and lateral direction are assumed to be proportional to the friction coefficient μ_{max_j}

$$F_{H_j} = \sqrt{F_{Wx_j}^2 + F_{Wy_j}^2} = \mu_{max_j} \cdot F_{z_j}. \qquad (55)$$

6.3 Slip Computation

A measure of the amount of sliding motion that occurs between the tire and the road are the longitudinal slip κ_j and the lateral slip α_j. The relative motion in longitudinal direction is based on the difference in speed between the rolling motion of the wheel with the dynamic tire radius r_{dyn_j} and the translational velocity of the wheel center v_{Wx_j}

$$v_{diff_j} = v_{Wx_j} - \dot{\rho}_{W_j} \cdot r_{dyn_j}. \qquad (56)$$

In most driving maneuvers, the driver performs a vehicle intervention that abruptly changes the current driving state. This results in a deformation of the tire in the longitudinal direction u and in the lateral direction w. A stationary state only sets in with time delay. This behavior is approximated by a first-order lag behavior. The resulting equations are

$$\sigma_{\kappa_j} \cdot \frac{du_j}{dt} + |v_{Wx_j}| \cdot u_j = -\sigma_{\kappa_j} \cdot v_{diff_j} \qquad (57)$$

$$\sigma_{\alpha_j} \cdot \frac{dw_j}{dt} + |v_{Wx_j}| \cdot w_j = \sigma_{\alpha_j} \cdot v_{Wy_j}. \qquad (58)$$

The relaxation lengths σ_{κ_j} and σ_{α_j} can be determined using the parameters of the tire model Magic Formula (Pacejka and Besselink, 2012). The longitudinal slip κ_j and the lateral slip α_j can be specified from the solution of the differential equations (57) and (58).

$$\kappa_j = \frac{u_j}{\sigma_{\kappa_j}} \cdot sgn(v_{diff_j}) \qquad (59)$$

$$\alpha_j = atan\left(\frac{w_j}{\sigma_{\alpha_j}}\right) \qquad (60)$$

6.4 Tire Model Magic Formula

After the kinematics of the tire-road contact is known by the two slip variables, the effective forces and torques in the contact area should now be calculated. Therefore, a model of the tire behavior is needed. On the one hand there are physical tire models like (Gipser, 2007) and (Baecker et al., 2010), which take into account the processes in the tire and therefore require a long computing time. On the other hand, there are empirical models like (Hirschberg et al., 2007) and (Pacejka and Besselink, 2012). These attempt to describe the characteristics measured on a tire test bench using mathematical approaches that are preferably composed of algebraic or trigonometric functions without taking the physical properties of the tire into account. This ensures that significantly less computation time is needed and a real-time computation is much easier to realize. Consequently, the empirical tire model Magic Formula is used here. It is widespread and offers a variety of key figures and influencing factors that allow a good approximation to the real tire behavior. In the following, only a rough overview is given and the basic structure is presented. Further information and all the equations needed for the computation of the individual parameters described here can be found in (Pacejka and Besselink, 2012).
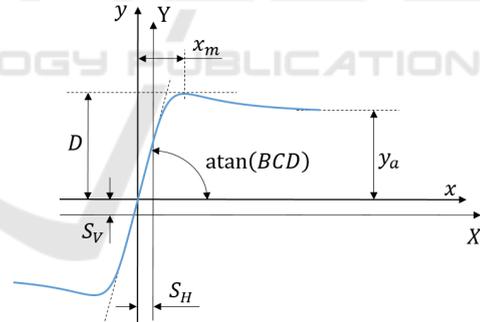

Figure 5: Tire behavior.

The Magic Formula model uses a mathematical approach to describe the tire forces and torques based on the trigonometric functions sine and arctangent. A realistic approximation of a measured curve is achieved by a suitable choice of the parameters B, C, D, E. These values take into account various influencing factors such as a variation of the wheel load F_z, camber γ, longitudinal slip κ and lateral slip α. The basic equation of the Magic Formula is

$$y = D \cdot \sin\left[C \cdot \arctan\left(B \cdot x - E \cdot (B \cdot x - \arctan(B \cdot x))\right)\right]. \qquad (61)$$

The characteristic curve in figure 5 may be shifted around the origin due to asymmetries in the tire structure

$$X = x + S_H \quad Y = y + S_V. \tag{62}$$

The parameter D represents the maximum value of the tire characteristics. It depends on the wheel load and the friction coefficient. The product of the three parameters $B \cdot C \cdot D$ correlates with the slope of the curve at the origin. The shape factor C is calculated from the height of the asymptote y_a and influences the limit of the range of the sine function

$$C = 1 \pm \left(1 - \frac{2}{\pi} \cdot \arcsin\left(\frac{y_a}{D}\right) \right). \tag{63}$$

The parameter B determines the slope at the origin and therefore it is called stiffness factor. The value of E specifies the curvature at the maximum of the curve

$$E = \frac{B \cdot x_m - \tan\left(\frac{\pi}{2 \cdot C}\right)}{B \cdot x_m - \arctan(B \cdot x_m)}. \tag{64}$$

The longitudinal and lateral forces are not independent of each other, since the lateral slip has an influence on the longitudinal force and the longitudinal slip on the lateral force. This fact is taken into account by the weighting factors $G_{x\alpha}$ and $G_{y\kappa}$. This leads to the tire longitudinal force

$$F_{Wx} = G_{x\alpha} \cdot F_{Wx0} + S_{vx\alpha}. \tag{65}$$

The weighting factor $G_{x\alpha}$ is chosen to be one if there is no lateral slip

$$G_{x\alpha} = \frac{\cos\left(C_{x\alpha} \cdot \arctan\left(B_{x\alpha} \cdot (\alpha + S_{Hx\alpha})\right)\right)}{\cos\left(C_{x\alpha} \cdot \arctan\left(B_{x\alpha} \cdot S_{Hx\alpha}\right)\right)}. \tag{66}$$

F_{Wx0} represents the tire force, which appear for pure longitudinal slip. $S_{vx\alpha}$ describes the offset force. The same applies to the side force. This results in

$$F_{Wy} = G_{y\kappa} \cdot F_{Wy0} + S_{vy\kappa}; \tag{67}$$

$$G_{y\kappa} = \frac{\cos\left(C_{y\kappa} \cdot \arctan\left(B_{y\kappa} \cdot (\kappa + S_{Hy\kappa})\right)\right)}{\cos\left(C_{y\kappa} \cdot \arctan\left(B_{y\kappa} \cdot S_{Hy\kappa}\right)\right)}. \tag{68}$$

7 VALIDATION

In figure 6 the vehicle accelerates from $50\frac{km}{h}$ to $80\frac{km}{h}$. The presented parameters show a high correlation between the Matlab and the CarMaker model. The current position of the accelerator pedal, which is required as an input signal of the powertrain model, is extracted from CarMaker. At the beginning, the accelerator pedal position is constant for two seconds.

Thereafter, the value is increased to the maximum value 1 over a period of 0.8 seconds. The signal is then constant for about 4 seconds. After the gear change, it decreases again. The engine torque has a similar curve progression. Due to the exponent of 0.80, the calculation of the currently available torque in (38) results in a degressive course. The maximum relative error in the engine torque between the both models is about 3% and occurs when the driver starts accelerating. A reason for this is the dead time in the CarMaker System which is neglected in Matlab. If a engine speed of $3800\frac{1}{min}$ is reached, a gear change takes place. As a result, the velocity drops abruptly. The angular velocity shows a similar behavior as the longitudinal velocity.
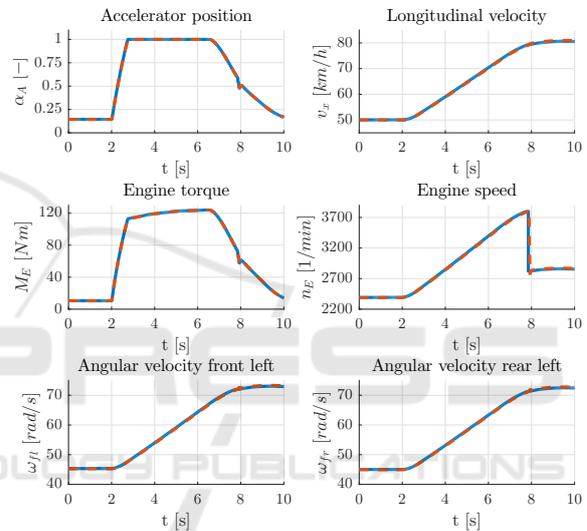

Figure 6: Validation of the powertrain model during an acceleration process: CarMaker (red); Matlab (blue).

The process of sinusoidal steering (cf. figure 7) starts after driving straight ahead for two seconds. The actual driving maneuver takes 14 seconds. The amplitude of the first half sine is half of the following three oscillation periods. If the steering angle were the same as the first one, the vehicle would drift off to one side because the direction of the vehicle would not be reversed. The curve progression of the wheel loads of the left and right front wheels behave symmetrically to the value that occurs in a pure longitudinal motion. The maximum relative error of the wheel load is about 1.5% und the absolute error is 45 N.

In order to obtain a stationary driving behavior, which is a prerequisite for a steady-state circular test, the vehicle in figure 8 drives straight ahead for 250 m. Then a circular path with a radius of 100 m is followed. Within ten seconds there is a smooth transition between the straight section and the circle. In this transitional period, the lateral acceleration increases and
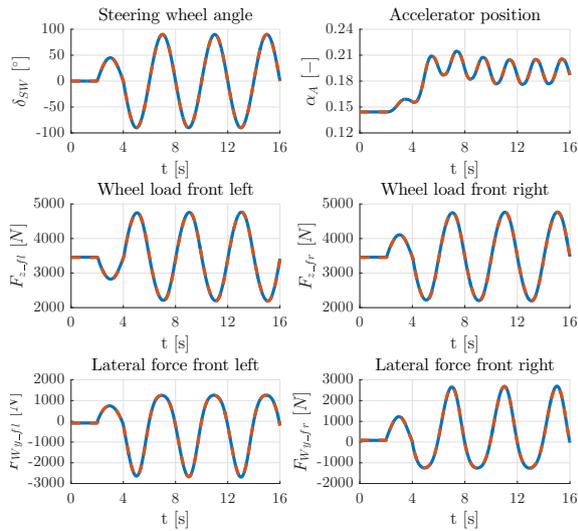
Figure 7: Validation of the tire forces during a sinusoidal steering: CarMaker (red); Matlab (blue).

Figure 8: Validation of the vehicle parameter during a circular test: CarMaker (red); Matlab (blue).

finally reaches a value of $2\frac{m}{s^2}$ in the CarMaker model, which remains the same over the entire period. In the Matlab model, the lateral acceleration is slightly increasing. The maximum occurring relative error is 3% and the absolute error is $0.06\frac{m}{s^2}$. The roll angle shows a similar behavior (relative error 2.8% and absolute error $4 \cdot 10^{-4} rad$). The yaw rate is almost the same in both models. Despite the deviations between the two models, there is no significant difference in the trajectory of the vehicle. This indicates a stable behavior of the Matlab model for the use in longer simulations.

Furthermore, the vehicle behavior is analyzed in an evasive maneuver (cf. 9). At the beginning, the vehicle is moving at a speed of $50\frac{km}{h}$ straight ahead. However, this is too fast to drive through the course. For this reason, a braking process is necessary. After the obstacle is avoided, the vehicle is accelerated again. The maximum absolute error occurring in the speed progression is $0.5\frac{km}{h}$ and the relative error 1.3%. The lateral acceleration shows only a visible deviation at 8.8 seconds (absolute error $0.1\frac{m}{s^2}$, relative error 4.0%). The difference is due to the fact that in the Matlab model the duration for the gear change is neglected. The roll angle and the yaw rate, however, show no difference.

Although the vehicle model has been validated only by comparison with a program system such as CarMaker, there are no limitations for the use in real-world simulations. The external influences like the wind are represented by the aerodynamics. The topography of the road is taken into account by the climbing resistance. The biggest uncertainties of the vehicle model are the parameters that occur in the
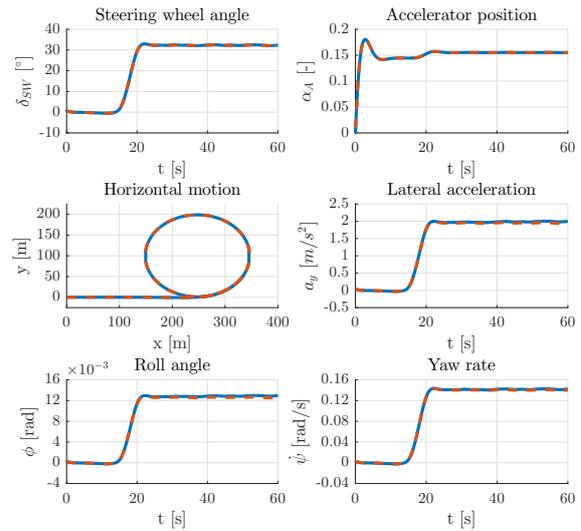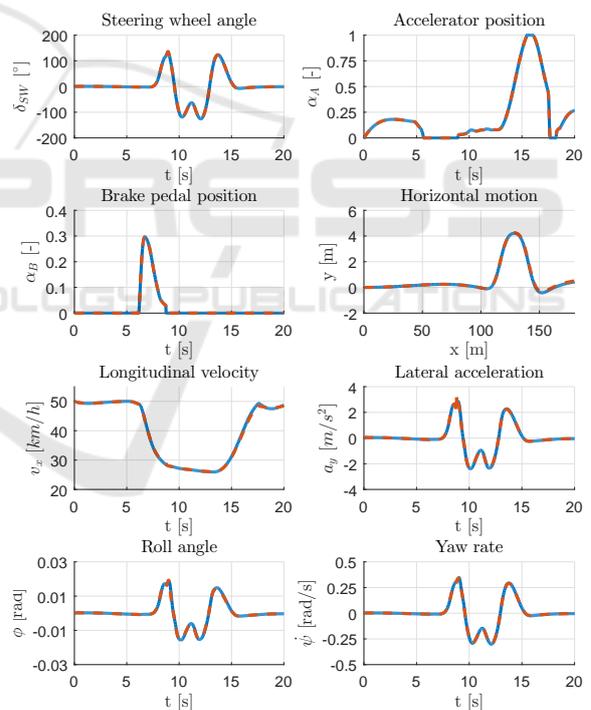

Figure 9: Validation of the vehicle parameter during an evasive maneuver: CarMaker (red); Matlab (blue).

single vehicle components. These have be determined experimentally on a test track before the vehicle model is used in real-world simulations.

8 PROGRAM STRUCTURE AND REAL-TIME CAPABILITY

When determining the structure of the source code, great emphasis was put on both computing speed and usability. The strucure of the vehicle model implemented in Matlab is shown in figure 10. In the main file, only the temporal change of the state vector is determined, which is described by the kinematic and dynamic equations of motion. Furthermore, the kinematics and dynamics in vector-matrix form are used to reduce the number of equations. The occurring parameters are determined in subroutines. The components described in the previous chapters, such as the powertrain or the tire model, are stored in separate files, so that they can easily be replaced if the vehicle configuration changes. Values such as the wheel load, which are required both for the calculation of the tire forces in the longitudinal and lateral direction and for the vertical motion of the wheel, are located in one of the upper program levels. Thereby, all program parts that need this information can access it and a recalculation is avoided. At the beginning the start values
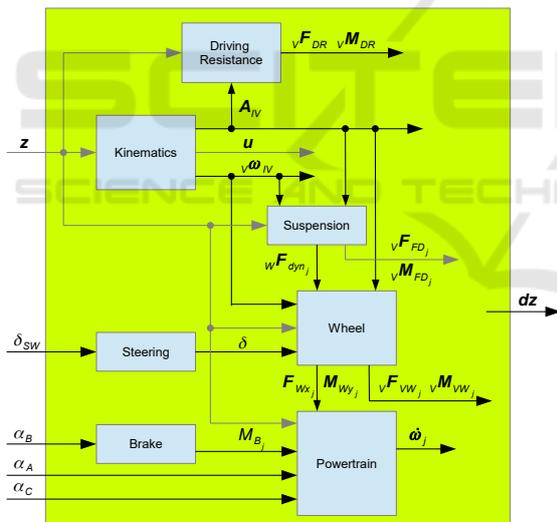

Figure 10: Structure of the Matlab model.

of the state vector z have to be defined. In addition, the temporal courses of the accelerator pedal position, the brake pedal position and the steering wheel angle are to be specified as input data for the vehicle model. At each time step, the change of the state vector dz is determined. This first order differential equation is then solved by means of the Matlab solver ode45 with a time increment of one millisecond. The state vector obtained thereby is the input for the next simulation step.

One of the fundamental conditions to the nonlinear

twin track model presented in this paper is the real-time capability. For this purpose, the computing time required for the maneuvers for validating the vehicle model is analyzed. To create the results listed in table 2, the mean of five simulations is calculated using a laptop with the characteristics(Intel (R) Core (TM) i5-7200U CPU)@ 2.50GHz 2.71GHz on a 64-bit Windows operating system. The results show that the vehicle dynamics model developed here enables a real-time simulation for all driving maneuvers presented here. In order to achieve a further reduction in

Table 2: Real-time capability.

Maneuver	Real	Matlab	mex
Acceleration [s]	10	2.72	0.46
Sinusoidal steering [s]	16	5.59	0.93
Circular test [s]	70	15.33	2.69
Evasive maneuver [s]	20	6.63	1.02

the computing time, the vehicle model is transferred to the C programming language. The resulting file is then integrated into Matlab as a mex file. The computing speed is increased by a factor of 5.7.

9 CONCLUSION

In this paper, a nonlinear twin track model has been introduced, containing all the components that are important for the vehicle handling. All components and the entire vehicle has been compared to the CarMaker system. The tire forces are validated by a sinusoidal steering. The powertrain has used an acceleration process for validation. All considered parameters show no significant difference between the both systems. The quality of the modeling of the behavior of the vehicle body, which also takes into account the vertical dynamics in addition to the horizontal dynamics, has been evaluated by a driving maneuver, which consists of a straight-ahead and a circular driving, and by an evasive maneuver. In the first one, there are small deviations in the roll angle and in the lateral acceleration, which are not constant during the circular driving and still increase slightly. In second maneuver one there is no difference. The computation time fulfills the requirement of a real-time simulation as a function of the illustrated maneuvers. The remaining computation time may be used in future projects to implement a controller that generates the required input variables of the vehicle model based on a predetermined trajectory and a speed profile. Furthermore, a method need to be developed to determine the required parameters of the nonlinear two-track model with reasonable effort on a proving ground.

ACKNOWLEDGEMENT

REFERENCES

Baecker, M., Gallrein, A., and Haga, H. (2010). A tire model for very large tire deformations and its application in very severe events. *SAE International Journal of Materials and Manufacturing*, 3(1):142–151.

Gillespie, T. D. (1992). *Fundamentals of vehicle dynamics*. Society of Automotive Engineers, Warrendale, PA, 4. printing edition.

Gipser, M. (2007). Ftire – the tire simulation model for all applications related to vehicle dynamics. *Vehicle System Dynamics*, 45(sup1):139–151.

Hirschberg, W., Rill, G., and Weinfurter, H. (2007). Tire model tmeasy. *Vehicle System Dynamics*, 45(sup1):101–119.

Pacejka, H. B. and Besselink, I. (2012). *Tire and vehicle dynamics*. Elsevier/BH, Amsterdam and Boston, 3rd ed. edition.

Popp, K. and Schiehlen, W. (1993). *Fahrzeugdynamik: Eine Einführung in die Dynamik des Systems Fahrzeug - Fahrweg ; mit 27 Beispielen*, volume 70 of *Leitfäden der angewandten Mathematik und Mechanik*. Teubner, Stuttgart.

Schramm, D., Hiller, M., and Bardini, R. (2018). *Vehicle Dynamics: Modeling and Simulation*. Springer, Berlin, Heidelberg and s.l., 2nd ed. 2018 edition.